Inorganic Chemistry

pubs.acs.org/IC

Article

Redox Potential Tuning of Dimolybdenum Systems through Systematic Substitution by Guanidinate Ligands

Nancy Rodríguez-López, Nathalie Metta, Alejandro J. Metta-Magana, and Dino Villagrán*

Cite This: *Inorg. Chem.* 2020, 59, 3091−3101

Read Online

ACCESS | Metrics & More | Article Recommendations | Supporting Information

ABSTRACT: We report the synthesis and characterization of a series of dimolybdenum paddlewheel complexes of the type $Mo_2(DAniF)_{4-n}(hpp)_n$ (n = 1−3), where DAniF is the anion of *N*,*N*′-di-*p*-anisyl-formamidine and hpp is the anion of 1,3,4,6,7,8-hexahydro-2*H*-pyrimido[1,2-*a*]pyrimidine. The effect on the electronic structure of these tetragonal paddlewheel dimolybdenum compounds was studied upon systematic substitution of formamidinate ligands by the more basic guanidinates. Mo−Mo distances in the paddlewheel structures decreased upon guanidinate ligand substitution, and were found to be 2.0844(6) and 2.0784(6), for $Mo_2(DAniF)_3(hpp)$ (**1**) and *trans*-$Mo_2(DAniF)_2(hpp)_2$ (**2**), respectively. Electrochemical studies show that the half-wave potential of the Mo_2^{5+}/Mo_2^{4+} couple shifts cathodically upon ancillary ligand substitution ranging from −0.286 V for the tetraformamidinate complex to −1.795 V for the tetraguanidinate analogue and with redox potentials of −0.75, −1.07, and −1.14 V for **1**, **2**, and **3** ($Mo_2(DAniF)(hpp)_3$), respectively. The presence of a second redox event assigned to the Mo_2^{6+}/Mo_2^{5+} couple was not observed until two guanidinate ligands were introduced. Raman spectroscopy shows that the ν(M−M) stretch gets systematically strengthened upon formamidinate ligand substitution by the guanidinate ligand hpp. The induced delta bond destabilization by the basic hpp ligand was measured using DFT calculations by tracking the energy of the frontier orbitals. The decrease in the HOMO−LUMO energy gap was supported by the red shift in the UV−vis spectra of the compounds: 412, 442, and 450 nm for **1**, **2**, and **3**, respectively.

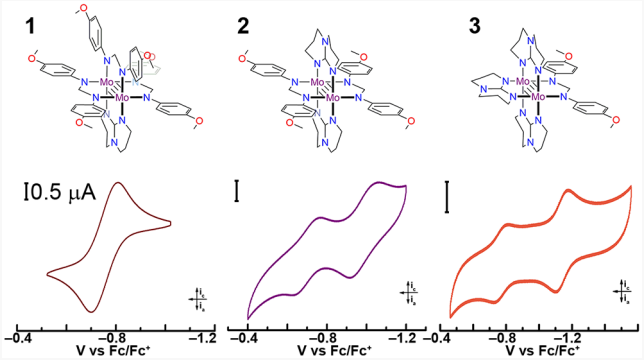

INTRODUCTION

The chemistry of metal−metal-bonded bimetallic complexes has been enhanced by the use of bidentate ligands such as carboxylates, amidinates, and guanidinates.[1] The nature of such supporting ligands has a strong effect on the oxidation states, redox potentials, and electronic properties of these compounds.[2,3] The increased attention to guanidinate ligands is a result of their capability to stabilize higher oxidation states in bimetallic complexes.[4−10] This ability is a result of the delocalization of the charge across the guanidinate backbone.[11,12] Of special interest is the bicyclic hpp ligand (hpp is the anion of 1,3,4,6,7,8-hexahydro-2*H*-pyrimido[1,2-*a*]pyrimidine) due to its high Lewis basicity (Scheme 1),[13,14] which allows the stabilization of the most easily ionizable family of complexes. $W_2(hpp)_4$, $W_2(TMhpp)_4$, and $W_2(TEhpp)_4$ present onset photoelectron ionization energies (3.51, 3.45, and 3.40 eV respectively) lower than the ionization energy for the cesium atom (3.89 eV).[1,15,16] The low ionization energies for compounds containing hpp have been associated with the strong antibonding interaction between the π orbitals of the ligand and the δ orbitals of the M_2^{4+} unit,[15] therefore destabilizing the M_2^{4+} core and favoring the oxidation to M_2^{5+} and M_2^{6+} species.[13,17,18] Consequently, large cathodic shifts in the redox potentials of bimetallic compounds of the M_2L_4 type are observed when the hpp ligand is introduced into the system.[1]

Scheme 1. Structural Ligands Used in Multiple Bonded Bimetallic Complexes in This Study: Carboxylate, Formamidinate, and Guanidinate Ligands

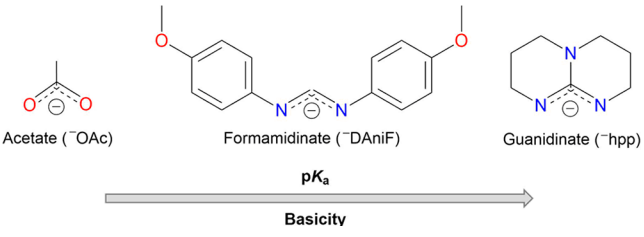

Research on bicyclic guanidinate ligands has centered on enhancing the solubility of bimetallic complexes in a variety of organic solvents[16,18] as well as fine-tuning their electronic and

Received: November 25, 2019
Published: February 18, 2020

electrochemical properties.[19,20] The individual effect of the ligands on the electronic properties of the system has been explored in similar bimetallic complexes by systematic replacement of the ancillary ligands.[21,22] Prior work with carboxylate and formamidinate ligands in dimolybdenum complexes has revealed that when carboxylates are systematically replaced by formamidinate ligands there is an increase in the stability of the oxidized species as well as a shift in the reduction potentials.[23] Previous results show a remarkable capacity of hpp to fine-tune the redox potential of the Mo_2^{4+} unit in M_2L_4 complexes. When bicyclic guanidinates are introduced into dimolybdenum paddlewheel complexes, the most stable species is the triply bonded Mo_2^{6+}.[8] Nonetheless, a study where formamidinates are systematically replaced by guanidinate ligands has not been reported. Thus, the effect of the substitution on the electronic structure and reduction potentials of the dimolybdenum center has not been explored.

Herein we report the synthesis, characterization, and study of a series of compounds of the form $Mo_2(DAniF)_{4-n}(hpp)_n$, where n = 1, 2, 3. We have synthesized and characterized dimolybdenum paddlewheel units with different proportions of formamidinate and guanidinate ligands in an attempt to fine-tune the electronic structure of these compounds and to gain a better understanding of the electron-donor properties of basic ligands such as acetates, formamidinates, and guanidinates when attached to a bimetallic system. The degree of tuning was quantified by exploring their electrochemical properties and comparing their prospective redox potentials, Raman shifts, and electronic absorption. Density functional theory (DFT) studies were performed to compare the respective energies of the compounds and to understand their electronic structure. The effect of ligand substitution on the electronic structures of the dimetal core was investigated using X-ray diffraction, electrochemistry, Raman, and UV−vis spectroscopies and were correlated with the results from DFT calculations.

EXPERIMENTAL SECTION

General Procedures. All synthesis and material handling procedures were conducted under an N_2 atmosphere using a drybox or standard Schlenk techniques, unless otherwise noted. All of the used solvents were dried and degassed using a Pure Process Technology solvent purification system. The materials used for this study: HDAniF,[24] $Mo_2(O_2CCH_3)_4$ (**I**),[25] $Mo_2(DAniF)_3(O_2CCH_3)$ (**II**),[26] $Mo_2(DAniF)_4$ (**III**),[27] *trans*-$Mo_2(DAniF)_2(O_2CCH_3)_2$,[21] and $[Mo_2(DAniF)(CH_3CN)_6](BF_4)_3$[22] were prepared following literature procedures. 1,3,4,6,7,8-Hexahydro-2*H*-pyrimido[1,2-*a*]pyrimidine (Hhpp) and other commercially available chemicals were used as received.

Physical Measurements. Elemental analyses were performed by Midwestern Microlab, LLC (Indianapolis, IN) and Galbraith Laboratories, Inc. (Knoxville, TN). UV−vis spectra were collected on a SEC2000 Spectra System with Visual Spectra 2.1 software from 350 to 800 nm. Infrared spectra were recorded on an Agilent Cary 630 FTIR spectrometer. Raman spectra were obtained on a Thermo Scientific DXR SmartRaman spectrometer using a 532 nm laser. ^{1}H NMR spectra were recorded on Bruker 300 and 400 MHz NMR spectrometers with chemical shifts referenced to the residual protic signal of C_6D_6. Electrochemical analyses by cyclic voltammetry (CV) were performed in THF using a CHI760D potentiostat with a Pt working electrode, Pt mesh auxiliary electrode, Ag/Ag^+ reference electrode, a scan rate of 100 mV/s, and 0.1 M $TBAPF_6$ as an electrolyte. Ferrocene was added at the end of the run as an internal standard.

X-ray Structure Determination. Suitable crystals for X-ray diffraction were prepared by the diffusion of hexanes into THF solutions of **1** and **2**. Each crystal was mounted with a small amount of silicone grease and centered in the goniometer of a Bruker SMART APEX CCD system equipped with a graphite monochromator and a Mo Kα fine-focus tube (λ = 0.71073 Å). Data for all crystals was collected at 100 K with no crystal decay observed during the collection. The frames were integrated with the Bruker SAINT Software package using a narrow-frame algorithm. Data was corrected for absorption effects via the multiscan method (SADABS). All structures were solved and refined by direct methods using the Bruker SHELXTL software package. The Mo−Mo distances for **1** and **2** are given in Table 1, while their crystallographic data are listed in Table 2.

Table 1. Experimental and Calculated Mo−Mo Bond Lengths (Å) for Compounds I−IV and 1−3

	experimental	calculated
I	2.0934(8)[40]	
II	2.0892(8)[12]	
III	2.0964(5)[13]	
1	2.0831(4)	2.12328
2	2.0784(6)[a]	2.11451
3		2.10730
IV	2.067(1)[1]	

[a]Isolation of the singly oxidized Mo_2^{5+} compound, **2**·PF_6, rendered a Mo−Mo distance of 2.114(2) Å, corresponding to the decrease in bond order from 4 to 3.5. See the SI for complete crystallographic information.

Table 2. X-ray Crystallographic Data for 1 and 2

	$Mo_2(DAniF)_3(hpp)$, **1**	*trans*-$Mo_2(DAniF)_2(hpp)_2$, **2**
formula	$C_{52}H_{57}Mo_2N_9O_6$	$C_{44}H_{52}Mo_2N_{10}O_4$
FW, g·mol^{-1}	1095.94	976.83
crystal system	monoclinic	triclinic
space group	$P2_1/c$	$P\bar{1}$
a (Å)	36.359(3)	9.7483(7)
b (Å)	12.0642(8)	10.6331(7)
c (Å)	23.0343(16)	11.4180(8)
α (deg)	90	65.7350(10)
β (deg)	106.0600(10)	86.1570(10)
γ (deg)	90	74.3210(10)
V (Å^3)	9709.5(11)	1037.51(12)
Z	8	1
d_{calc} (g·cm^{-3})	1.499	1.563
μ (mm^{-1})	0.577	0.662
2θ (deg)	1.17−31.00	1.96−27.43
λ, Å	0.71073	0.71073
T, K	100(2)	100(2)
GOF	0.951	1.036
R1,[a] wR2($I > 2\sigma(I)$)[b]	0.0535, 0.1210	0.0483, 0.1072

[a]$R1 = \sum||F_o| - |F_c||/\sum|F_o|$. [b]$wR2 = [\sum[w(F_o^2 - F_c^2)^2]/\sum w(F_o^2)^2]^{1/2}$, $w = 1/[\sigma^2(F_o^2) + (aP)^2 + bP]$, where $P = [\max(F_o^2 \text{ or } 0) + 2(F_c^2)]/3$.

$Mo_2(DAniF)_3(hpp)$ (1). A mixture of yellow $Mo_2(DAniF)_3(O_2CCH_3)$ (1.02 g, 1.00 mmol) and Hhpp (0.139 g, 1.00 mmol) was dissolved in 40 mL of THF. While the mixture was stirred, 2 mL of a 0.5 M solution of $NaOCH_3$ in methanol were slowly added. The color first turned red and then brown. The reaction was stirred for 5 h at room temperature, producing white crystalline sodium acetate. After removal of the solvent under reduced pressure, the residue was extracted with 20 mL of

https://dx.doi.org/10.1021/acs.inorgchem.9b03394
Inorg. Chem. 2020, 59, 3091−3101

Scheme 2. Reaction Conditions for the Procurement of Compounds 1−3[a]

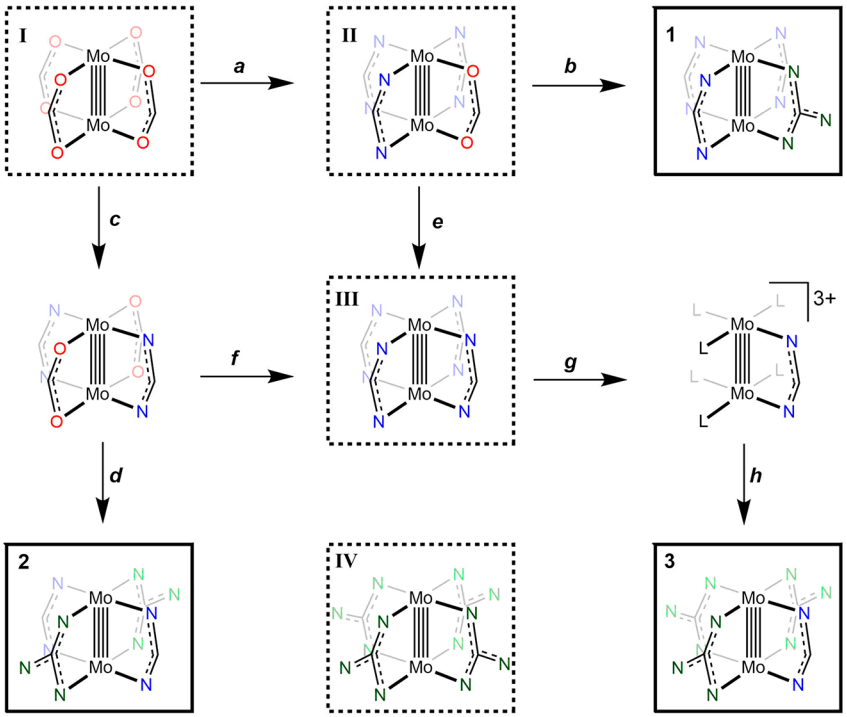

[a](a) Mixing **I** with 3 equiv of HDAniF and $NaOCH_3$ in THF; (b) reaction of **II** with 1 equiv of Hhpp and $NaOCH_3$ in THF; (c) addition of 2 equiv of HDAniF and $NaOCH_3$ to **I** in THF; (d) addition of 2 equiv of Hhpp and $NaOCH_3$ in THF to *trans*-$Mo_2(DAniF)_2(O_2CCH_3)_2$; (e) reaction of **II** with 1 equiv of HDAniF and $NaOCH_3$ in THF; (f) reaction of *trans*-$Mo_2(DAniF)_2(O_2CCH_3)_2$ with 2 equiv of HDAniF and $NaOCH_3$ in THF; (g) mixing **III** with 3 equiv of HBF_4 in CH_3CN:DCM; (h) addition of 3 equiv of Hhpp and $NaOCH_3$ to $[Mo_2(DAniF)(CH_3CN)_6](BF_4)_3$ in THF. The tetraguanidinate (**IV**) is obtained by the reaction of $Mo_2(O_2CF_3)_4$ with 4 equiv of Hhpp in THF. Compounds **1−3** are allocated in bold line boxes, while other compared compounds (**I−IV**) can be found in dashed line boxes. Letters O and N are used to represent the oxygen and nitrogen atoms in the acetates, formamidinates, and guanidinates ligands, while L refers to an acetonitrile molecule. All reactions were carried out under an inert atmosphere at room temperature unless otherwise noted.

dichloromethane; filtration removed NaO_2CCH_3. The volume of the filtrate was reduced to about 5 mL with vacuum evaporation. Ethanol (10 mL) was added to the residue with vigorous stirring. A bright-yellow solid and a dark-brown supernatant solution were obtained. After decantation, the solid was washed with ethanol (2 × 10 mL), followed by 10 mL of hexanes, and dried under vacuum. Yield: 901 mg, 82%. ^{1}H NMR (δ in C_6D_6): 1.75 (q, 4H, $-2CH_2$), 2.89 (t, 4H, $-2CH_2$), 3.21 (s, 6H, $-OCH_3$) 3.22 (s, 12H, $-OCH_3$), 3.45 (t, 4H, $2CH_2$), 6.58 (d, 8H, aromatic C−*H*) 6.67 (d, 16H, aromatic C−*H*), 8.56 (s, 2H, −NC*H*N−), 8.58 (s, 1H, −NC*H*N−). UV−vis λ_{max}: 412 nm. Raman (cm^{-1}): ν = 487. ESI-MS (m/z): calcd 1097.3 [M + H^+], found 1097.5 [M + H^+]. Anal. Calcd for $Mo_2C_{52}N_9O_6H_{57}$: C, 56.99; N, 11.5; H, 5.24. Found: C, 56.79; N, 11.27; H, 5.35.

***trans*-$Mo_2(DAniF)_2(hpp)_2$, 2.** A mixture of yellow trans-$Mo_2(DAniF)_2(O_2CCH_3)_2$ (0.500 g, 0.610 mmol) and Hhpp (0.160 g, 1.15 mmol) was dissolved in 40 mL of THF. While the solution was stirred, 2.30 mL of a 0.5 M solution of $NaOCH_3$ in methanol were slowly added. The color turned orange, and with further stirring the solution turned a brighter shade of orange. The reaction was stirred for 5 h. After 5 h, the stirring was stopped and the solution was allowed to settle. An orange solid and a dark brown supernatant solution were obtained. After decantation, the solid was washed with diethyl ether (2 × 10 mL) and dried under vacuum. Yield: 495 mg, 83%. ^{1}H NMR (δ in C_6D_6): 1.79 (q, 8H, $-2CH_2$), 2.92 (t, 8H, $-2CH_2$), 3.29 (s, 12H, $-OCH_3$), 3.59 (t, 8H, $-2CH_2$), 6.62 (d, 8H, aromatic C−*H*), 6.74 (d, 8H, aromatic C−*H*), 8.41 (s, 2H, −NC*H*N−). UV−vis λ_{max}: 442 nm. Raman (cm^{-1}): ν = 494. ESI-MS (m/z): calcd 980.24 [M + H^+], found 980.5 [M + H^+]. Anal. Calcd for $Mo_2C_{44}N_{10}O_4H_{54}$: C, 53.99; N, 14.31; H, 5.56. Found: C, 53.81; N, 14.07; H, 5.47. ESI-MS: m/z: 982.40.

$Mo_2(DAniF)(hpp)_3$ (3). To a mixture of purple $[Mo_2(DAniF)(CH_3CN)_6](BF_4)_3$ (0.600 g, 0.650 mmol) and Hhpp (0.270 g, 1.95 mmol) in THF, $NaOCH_3$ (3.90 mL) 0.5 M in methanol was added dropwise. The color turned bright orange upon addition of the sodium salt. The reaction was stirred for 5 h. After 5 h, the stirring was stopped and the solution was allowed to settle. An orange solid could be seen at the bottom, and the supernatant was decanted. The solid was washed with diethyl ether (2 × 10 mL) and dried under vacuum. Yield: 395 mg, 73%. ^{1}H NMR (δ in C_6D_6): 1.53 (q, 8H, $-2CH_2$), 2.58 (t, 8H, $-2CH_2$), 2.89 (t, 4H, $-2CH_2$), 2.92 (q, 4H, $-2CH_2$), 3.10 (t, 8H, $-2CH_2$), 3.33(s, 6H, $-OCH_3$), 3.46, (t, 4H, $-2CH_2$), 6.62 (d, 4H, aromatic C−*H*), 6.77 (d, 4H, aromatic C−*H*), 8.33 (s, 1H, −NC*H*N−). UV−vis λ_{max}: 450 nm. Raman (cm^{-1}): ν = 505. ESI-MS (m/z): calcd 822.2 [M − $2OCH_3$ + Na^+], found 821.9 [M − $2OCH_3$ + Na^+].

COMPUTATIONAL DETAILS

Density functional theory (DFT) calculations were performed with the hybrid Becke-3 parameter exchange functional and the Lee−Yang−Parr nonlocal correlation functional (B3LYP)[28,29] as implemented by the *Gaussian 09*[30] (Revision C.01) program suit. A double-ζ-quality basis set (cc-pvdz)[31−35] was used on nonmetal atoms (carbon, nitrogen, oxygen, and hydrogen). An effective core potential (ECP) representing the $1s^2s^2p^3s^3p^3d^4p$ core was employed for the molybdenum atoms, along with the associated double-ζ basis set (LANL2DZ).[36−39] The absence of imaginary vibrations in the frequency calculations for all compounds indicated that the gas-phase geometry optimizations were minima in the

https://dx.doi.org/10.1021/acs.inorgchem.9b03394
Inorg. Chem. 2020, 59, 3091−3101

potential energy surface. Polarizability derivatives (Raman intensities) were computed using the keyword Freq = Raman in the Gaussian 09 package. Time-dependent density functional theory (TD-DFT) was used to calculate the electronic transition energies for the 15 lowest singlet excited states of all neutral compounds.[40−46] All calculations were performed in a 44-processor PowerWolf PSSC supercomputer cluster running Linux Red Hat 4.1.2-54 located at the University of Texas at El Paso. Isosurface plots of frontier molecular orbitals were generated using Avogadro software with isodensity values of 0.04.

RESULTS AND DISCUSSION

Molecular Design and Syntheses. Redox tuning can be studied through ligand substitution by taking advantage of the well-defined redox properties of quadruply bonded Mo_2 complexes. An overview of the synthetic routes followed for the synthesis of all involved compounds is shown in Scheme 2, where **1**−**3** are placed in bold line boxes. Other species compared in the study are written off as **I**−**IV** and can be found in dashed line boxes. The depicted reactions are listed with italicized lowercase letters *a*−*h*. Letters O and N are used to represent the oxygen and nitrogen atoms found in the ancillary ligands (acetates, formamidinates, and guanidinates), while L refers to an acetonitrile molecule in an equatorial position. A brief description of the reactions for the synthesis of each species can be found in the footnote associated with Scheme 2. The use of carboxylates and formamidinate ligands allows compounds bearing different patterns of ancillary ligands: one carboxylate and three formamidinates as well as two carboxylates and two formamidinates in either the cis or trans configuration. The remaining carboxylates in such precursors could be replaced by the more basic guanidinates to afford the anticipated compounds.

As reported,[25] starting material $Mo_2(O_2CCH_3)_4$ (**I**) can be used to synthesize $Mo_2(DAniF)_3(O_2CCH_3)$ (**II**). The stoichiometric addition of the more basic formamidinate ligand (HDAniF) compared to acetate allows their substitution to afford **II** (Scheme 2, route *a*). Compound **1** was synthesized by replacing the acetate ligand in **II** with the bicyclic guanidinate hpp (Scheme 2, following conditions in *b*). $Mo_2(DAniF)_3(hpp)$ (**1**) was obtained in 82% yield as a yellow powder. Compound **1** is considerably stable as a solid under an inert atmosphere. It does not react with chlorinated solvents, and it is soluble in donor solvents such as THF as well as aromatic solvents such as benzene.

The synthesis of trans isomer $Mo_2(DAniF)_2(hpp)_2$ (**2**) was performed similarly to **1**. Precise control of the stoichiometry for the synthesis of precursor *trans*-$Mo_2(DAniF)_2(O_2CCH_3)_2$ was crucial (Scheme 2, conditions in *c*). Excess of formamidinate would otherwise react to yield **III**. Once the precursor was successfully obtained, the replacement of the acetate ligands by hpp was completed (Scheme 2, following reaction conditions in *d*). *trans*-$Mo_2(DAniF)_2(O_2CCH_3)_2$ (**2**) was obtained as an orange powder in 83% yield. Compound **2** is stable in the solid state under an inert atmosphere. It reacts with chlorinated solvents and is only partially soluble in other solvents. While we were not able to obtain the cis isomer, no interconversion from the trans to cis configuration was detected.

In contrast to the direct synthetic pathway of **1** and **2**, $Mo_2(DAniF)(hpp)_3$ (**3**) was prepared through an indirect route (Scheme 2). In order to afford **3**, precursor $[Mo_2(DAniF)(CH_3CN)_6]^{3+}$ was first obtained by reacting tetrafluoroboric acid, HBF_4, and $Mo_2(DAniF)_4$ (**III**) (Scheme 2, reaction conditions in *g*).[27] The removal of formamidinates is more difficult compared to the displacement of acetate groups in **I** due to their increased basicity. Their substitution requires stronger reactants (HBF_4) than $NaOCH_3$ used in the displacement of acetates in **I**. Compounds with the formula $Mo_2(DAniF)_{4-n}(CH_3CN_{eq})_{2n}$, are useful since acetonitrile molecules can be easily displaced in substitution reactions.[21] In the substitution of $^-$DAniF by CH_3CN, HBF_4 protonates the formamidinate ligand to a monodentate intermediate, while a neutral acetonitrile occupies the open coordination site.[22] Finally, the MeCN ligands are substituted by hpp to obtain $Mo_2(hpp)_3(DAniF)$ (**3**) as an orange powder in 73% yield (Scheme 2, reaction *h*). This compound is partially soluble in most donor and aromatic solvents and is highly air-sensitive.

Structural Determinations. Single crystals suitable for crystallography were obtained by the diffusion of hexanes into a THF solution of the compounds. The structures of **1** and **2** provided in Figure 1 show a paddlewheel structure with

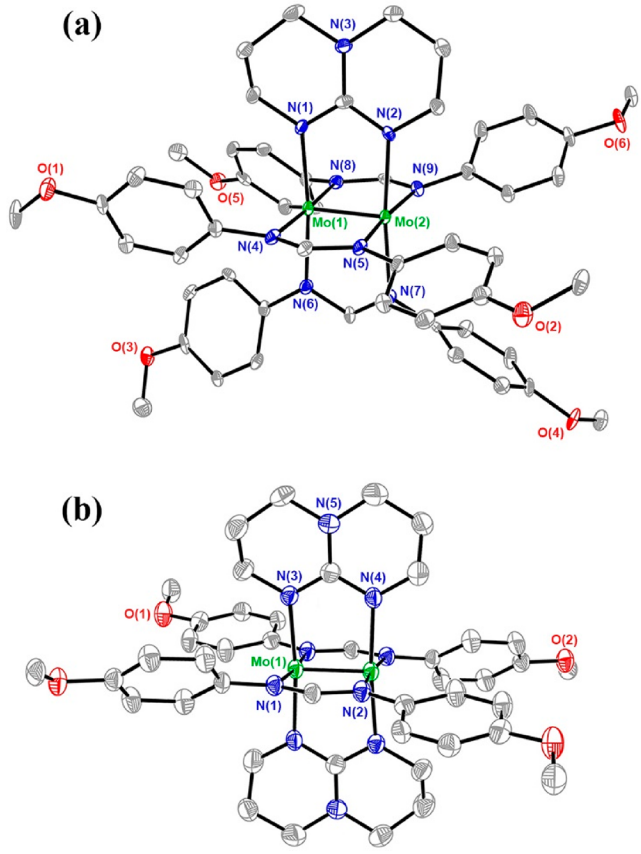

Figure 1. Crystal structures for **1** and **2** with ellipsoids drawn at the 50% probability level. All hydrogen atoms have been omitted for clarity.

formamidinate and guanidinate structural ligands. Figure 1a shows the molecular structure of $Mo_2(DAniF)_3(hpp)$ (**1**) with selected bond distances and angles given in Table S1. Compound **1** crystallizes in monoclinic space group $P2_1/c$ with Z = 8. The M−M dimolybdenum bond distance 2.0831(4) Å, falls in the range of 2.06−2.17 Å, which corresponds to that of a typical Mo_2 quadruple bonded

https://dx.doi.org/10.1021/acs.inorgchem.9b03394
Inorg. Chem. 2020, 59, 3091−3101

compound.[47,48] The replacement of the acetate ligand in starting material $Mo_2(DAniF)_3(O_2CCH_3)$ (**II**) by the guanidinate ligand to form **1** was shown to affect the metal−metal bond distance. Compared to the reported Mo−Mo bond in **II**, of 2.0892(8) Å, the metal−metal distance was shortened by 0.0061 Å. The Mo−N_{hpp} bond distance in **1** is on average 2.1315 Å, while the average bond lengths for formamidinate nitrogen atoms Mo−N_{trans} and Mo−N_{cis} are 2.1605 and 2.1532 Å, respectively. The bond distances found trans to guanidinate nitrogen atoms are slightly longer than those cis to them. This lengthening trend of trans groups is similar to the trans influence of both guanidinate and formamidinate groups relative to carboxylates.[21,49,50] Meanwhile, the average N−C bond lengths were 1.357 Å for $^-$hpp and 1.331 Å for $^-$DAniF, which are consistent with the delocalized charge in these bonds.

Compound **2**, where two guanidinates in the trans configuration have been introduced into the system, crystallizes in the triclinic space group $P\bar{1}$. The molecule occupies a special position (Z = 1) having the center of the M−M bond sit on an inversion point. Therefore, the two Mo(DAniF)(hpp) half-units are crystallographically equivalent. Figure 1b shows the molecular structure for *trans*-$Mo_2(DAniF)_2(hpp)_2$ (**2**) with selected bond distances and angles given in Table S1. The Mo−Mo distance of 2.0784(6) Å is shorter than that in **1** by 0.006 Å as expected from the addition of a second hpp unit. The Mo−N_{hpp} bond distance in **2** is on average 2.138(3) Å, whereas that for Mo−N_{DAniF} is 2.158(3) Å. We were unable to obtain single crystals of **3** suitable for adequate data collection.

The C−N and C−C bond distances observed in the guanidinate ligands for complexes **1** and **2** are comparable. In addition, distances of 1.45 and 1.51 Å were observed for the C−N and C−C bonds in the formamidinate ligands, respectively. On the other hand, the two equivalent C−N bonds of the CN_3 unit are shorter, with a bond length of 1.34 Å. This observation is in agreement with the atoms in the hpp core allowing charge delocalization and causing the guanidine core to demonstrate planarity (178.9°). In addition, the shorter Mo−N_{hpp} distance for the hpp ligand when compared to the Mo−N distance for the formamidinate ligand is a reflection of the stronger binding of hpp due to the higher ligand basicity.

Electrochemical Studies. Dimolybdenum paddlewheel structures show one-electron oxidations that leads to the formation of a Mo_2^{5+} unit.[51] However, when hpp is used as a ligand in $Mo_2(hpp)_4$ (**IV**), two one-electron oxidations are observed.[8] Thus, to understand the ability of hpp to stabilize higher oxidation states the electrochemical properties of **I**, **II**, and **III** and **1**, **2**, and **3** were studied. Cyclic voltammograms (CV) for the studied compounds and their precursors are depicted in Figure 2 and Figure S8, respectively. Electrochemical data for the compounds presented in this work as well as precursors **I**, **II**, **III**, and **IV** are given in Table 3, and all redox potentials have been referenced against the ferrocene/ferrocenium couple (Fc/Fc^+). Compound **I** shows a one-electron reversible event with a half-wave potential ($E_{1/2}$) at −0.120 V, which corresponds to the reversible oxidation of Mo_2^{4+} to Mo_2^{5+}. Similarly, **II** and **III** display a one-electron oxidation with $E_{1/2}$ = −0.286 and −0.381 V, respectively. The replacement of one formamidinate by a guanidinate ligand in **1** shifts the Mo_2^{4+} to Mo_2^{5+} oxidation potential by 0.5 V in the negative direction ($E_{1/2}$ = −0.754 V vs Fc/Fc^+) when compared to **II** and **III**. The lower oxidation potential of **1** is expected due to the increase in the electron density on the metal center as a result of the increased Lewis basicity of hpp.[14]

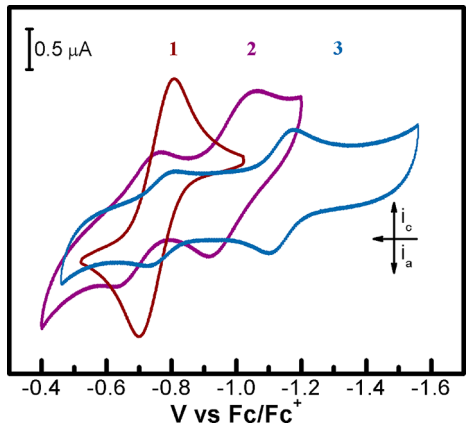

Figure 2. Cyclic voltammograms for **1**, **2**, and **3** (1 mM) in THF with potentials referenced to Fc/Fc^+. The electrochemical analyses were performed with Pt working and auxiliary electrodes and an Ag/AgCl reference electrode, with 0.1 M $TBAPF_6$ as the electrolyte and a scan rate of 100 mV/s. The poor solubility of **2** and **3** is reflected in the decreased current response.

Table 3. Redox Potentials in Volts (vs Fc/Fc^+) for Mo_2L_4 Compounds I−IV and 1−3

	$E_{1/2}^2$ (Mo_2^{6+}/Mo_2^{5+})	$E_{1/2}^2$ (Mo_2^{5+}/Mo_2^{4+})
I		−0.120
II		−0.286
III		−0.381[24]
1		−0.754
2	−0.693	−0.988
3	−0.763	−1.136
IV	−0.968[7]	−1.795[7]

The bicyclic guanidinate, hpp, has shown the ability to stabilize higher oxidation states in bimetallic complexes due to its π-donor nature and increased basicity.[16,52] The CV for $Mo_2(hpp)_4$ (**IV**) shows two reversible one-electron redox events at $E_{1/2}$ (1) = −1.795 V and $E_{1/2}$ (2) = −0.968 V corresponding to the oxidation of Mo_2^{4+} to $Mo_2^{5+}$and Mo_2^{5+} to Mo_2^{6+}, respectively.[8] The charge stabilization ability of hpp can be observed when a second guanidinate is introduced in **2**. Two one-electron reversible redox processes are obtained at $E_{1/2}$ (1) = −0.988 V and $E_{1/2}$ (2) = −0.693 V, analogous to those for **IV**. The half-wave potentials, $E_{1/2}$ (1) and $E_{1/2}$ (2), were assigned to the oxidation of Mo_2^{4+} to Mo_2^{5+} and Mo_2^{5+} to Mo_2^{6+}, respectively. The redox potential at −0.693 V (Figure 2) indicates that the oxidation of $\mathbf{2}^+$ is easier than that of **I** and **III**. The measured half-wave potential for the $[Mo_2]^{4+/5+}$ pair in **2** is significantly more negative than that of **1** by 0.234 V. To note, the decreased solubility of **2** compared to that of **I**, **II**, and **1** in THF causes a considerable decrease in the current in the cyclic voltammogram.

The replacement of a third formamidinate by hpp in **3** shows a similar voltammogram to that of **2**, with two one-electron reversible redox events at $E_{1/2}$ (1) = −1.136 V and $E_{1/2}$ (2) = −0.763 V vs Fc/Fc^+. Analogous to **2**, these processes correspond to the oxidation of Mo_2^{4+} to Mo_2^{5+} and Mo_2^{5+} to Mo_2^{6+}, respectively. The redox potential for the $[Mo_2]^{5+/4+}$ pair in **3** is 0.148 V more negative than in **2**. This

https://dx.doi.org/10.1021/acs.inorgchem.9b03394
Inorg. Chem. 2020, 59, 3091−3101

trend continues when the final formamidinate is replaced to get **IV** where the $E_{1/2}$ for the oxidation of Mo_2^{4+} to Mo_2^{5+} occurs at −1.795 V vs Fc/Fc^+. In addition, the low solubility of **3**, as observed for **2**, is reflected in the decreased redox current observed in Figure 2.

The systematic substitution of formamidinates by guanidinates allows to probe the ability of hpp to destabilize the quadruple bond. The measured $E_{1/2}$ for the Mo_2^{4+} to Mo_2^{5+} oxidation shifts cathodically as guanidinates are added to the Mo_2^{4+} unit. It is evident that the guanidinate ligand, hpp, tunes the redox potentials of these bimetallic molybdenum systems due to the high basicity of the anion along with its ability to interact strongly with the Mo_2^{n+} core via its delocalized π electrons in the central guanidinate core.[52] Therefore, the δ bonding orbital is destabilized upon increasing the electron-donating ability of the ancillary ligand. The redox properties of these series of compounds show the increase in basicity for $^-$OAc < $^-$DAniF < $^-$hpp, with guanidinate being the most basic. Consequently, the guanidinate ligands are the most difficult to substitute while acetates are the easiest ones due to their increased lability. Moreover, a trans influence is noticed proportionally to the basicity of the ligand, and such influence is also manifested in the Mo−N bond distance (Table S1).

Spectroscopic Properties. The UV−vis spectra of compounds **1**−**3** show two absorption peaks: one near the UV region (∼300 nm) and one in the visible region (∼450 nm). The low-energy transition in the region of 400−600 nm, assigned to Mo_2 $\delta \rightarrow Mo_2$ δ^*, has been well established in the literature for quadruply bonded paddlewheel dimolybdenum compounds.[22,53,54] The energy of this transition relies on the nature of the ancillary ligands.[55] The absorption spectra of **1**−**3** are shown in Figure 3. Compound **1** shows a band at 412

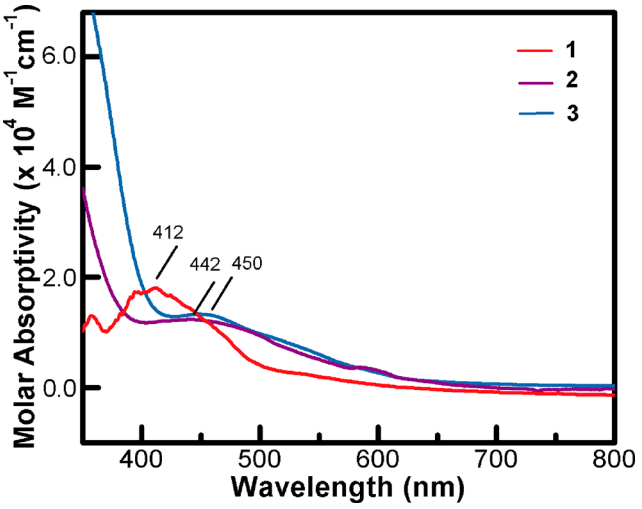

Figure 3. Electronic spectra of compounds **1** (λ_{max} = 412 nm; red spectrum), **2** (λ_{max} = 442 nm; purple spectrum), and **3** (λ_{max} = 450 nm; blue spectrum) in THF solution at room temperature.

nm, arising from the $\delta \rightarrow \delta^*$ transition. Similarly, compounds **2** and **3** presented a band at 442 and 450 nm, respectively. A detailed electronic transition analysis was performed using time-dependent density functional theory (TD-DFT) calculations (vide supra). Raman spectroscopy was used to further probe the electronic structure and the strength of the metal−metal bond in **1**−**3**. The spectra were obtained with laser excitation of 532 nm and are found in Figure 4. For nonaxially substituted carboxylate dimolybdenum complexes such as **I**,

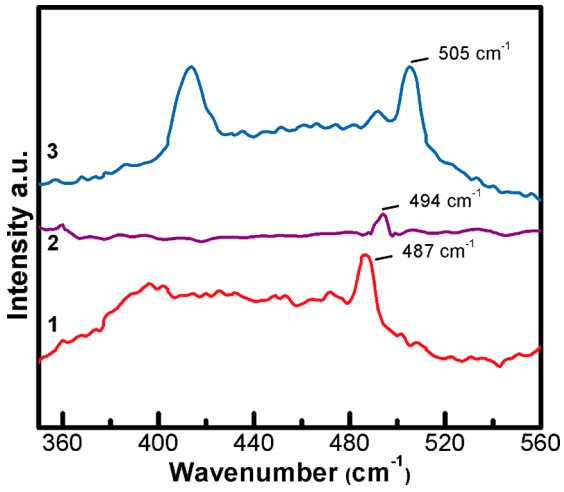

Figure 4. Raman spectra of compounds **1** (ν = 487 cm^{-1}, bottom trace), **2** (ν = 494 cm^{-1}, middle trace), and **3** (ν = 505 cm^{-1}, top trace) at room temperature.

the band associated with the symmetric ν(Mo−Mo) vibration appears at 404 cm^{-1} (Figure S9), while for the halide species it is 342 ± 8 cm^{-1}.[56] The strongest Raman signal was assigned to the Mo−Mo stretching mode as supported by DFT calculations. The ν(Mo−Mo) of **1** shows a Raman shift at 487 cm^{-1}. The trans isomer, **2**, has a Mo−Mo shift at 494 cm^{-1}. Finally, compound **3** has a Mo−Mo vibration at 505 cm^{-1}. This complex shows strong fluorescence, which accounts for the high intensity detected. The sequential addition of guanidinate ligands shifts the ν(Mo−Mo) Raman signal, this observation is consistent with the destabilization of the Mo−Mo bond due to the high basicity and electron-donating abilities of guanidinate ligands.[57]

DFT Calculations. Density functional theory (DFT) calculations were performed on precursors **III** and **IV**, and all synthesized compounds, **1**−**3**, to gain insight into the electronic structure of their Mo_2 cores, their ground-state geometries, and the nature of their frontier orbitals. The gas-phase geometry optimizations were performed using the crystal structure parameters as the starting point for the calculations. The calculated gas-phase Mo−Mo bond distance for **1** is 2.12328 Å, which is comparable to the experimentally obtained 2.0831(4) Å. For **2**, the DFT obtained metal−metal bond is 2.11451 Å while the experimental one is 2.0784(6) Å. Meanwhile, the calculated Mo−Mo bond for **3** is 2.10730 Å. There is a consistent overestimation of the Mo−Mo bond by about 0.04 Å, which has been well established in the literature when B3LYP and other functionals are employed.[16,58] The shortening of the M−M bond distance is consistent with the greater overlap of the δ bond due to the addition of guanidinates as ancillary ligands. This effect is described by the linear relationship of the M−M bond distance with the number of guanidinate ligands surrounding the bimetallic center (Figure 5). The fitting of the data gives a correlation coefficient of (R^2) 0.921. Another correlation is also observed between the energy of the $\delta \rightarrow \delta^*$ transition and the metal−metal bond distance. As the metal−metal bond length increases, the energy of the $\delta \rightarrow \delta^*$ transition increases as well.

https://dx.doi.org/10.1021/acs.inorgchem.9b03394
Inorg. Chem. 2020, 59, 3091−3101

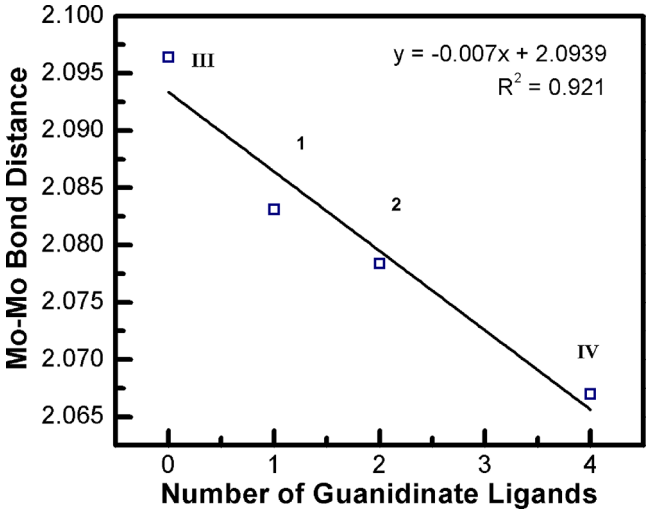

Figure 5. Plot of the dependence of the Mo−Mo bond distance on the number of guanidinates in **III**, **1**, **2**, and **IV**. The squares are the measured values, and the solid line is the least-squares fit of the data.

Figure 6 depicts the HOMO and LUMO orbitals for compounds **1**−**3**. The highest occupied molecular orbital

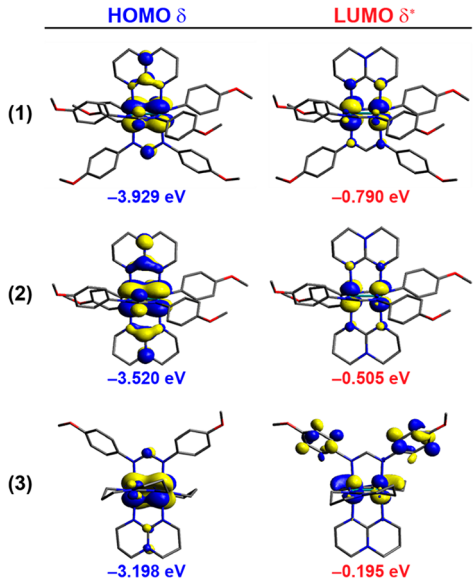

Figure 6. Illustration of the HOMO and LUMO for compounds **1**−**3** with 0.04 contour surfaces calculated with DFT.

(HOMO) for all of the compounds was established as a metal-based δ orbital with some degree of ligand mixing. The composition of the HOMO attributes the lower redox potential wave in the cyclic voltammograms for **1**−**3** to the $Mo_2^{5+/4+}$ process. On the other hand, the lowest unoccupied molecular orbital (LUMO) is a metal-based δ^* orbital, except in $Mo_2(hpp)_4$ where the LUMO is a metal-based σ^* while LUMO + 1 is the δ^*.[59] A molecular orbital diagram for the frontier molecular orbitals of the $Mo_2(DAniF)_{4-n}(hpp)_n$ (n = 0, 1, 2, 3, 4) molecules is given in Figure 7, which allows a comparison of relative energies for **III**, **1**, **2**, **3**, and **IV**. The highest HOMO energy observed was at −2.813 eV for $Mo_2(hpp)_4$ (**IV**), with 64% metal character, while the lowest and most stable orbital is that for $Mo_2(DAniF)_4$ (**III**) with an onset HOMO δ energy of −4.32 eV and 75% metal character.

The electronic structure of **1** shows that the HOMO (−3.929 eV) is metal-based (66%) with δ character. Contrary to typical paddlewheel complexes, the σ orbital is found to be less stable than the π orbitals, at −5.932 eV (HOMO−8). The HOMO−9 and HOMO−10 (at −5.997 eV and −6.156 eV, respectively) are the π orbitals showing the strong ligand interaction between the guanidinate N atoms and the metal center. The LUMO of **1** is the metal-based δ^* found at −0.790 eV. Compound **2** has an onset LUMO energy of −0.505 eV, which is 0.285 eV higher in energy than that for **1**. The Mo_2 unit makes the largest contribution to the HOMO with 65% at −3.520 eV. Similar to **1**, the σ orbital (HOMO−4) is less stable than the π orbitals at −5.515 eV. Finally, HOMO−9 and HOMO−11 are found at −5.921 and −6.027 eV, respectively. On the other hand, **3** has a HOMO energy of −3.198 eV. Interestingly, the metal character of the compound decreases again with respect to that of **1** and **2** to 64%. Once again, the σ orbital is found before the π orbitals at −5.290 eV (HOMO−4), while HOMO−5 and HOMO−8 are found at −5.516 and −5.655 eV, respectively. The reduction potentials for this series are linearly correlated to the number of guanidinates in the complexes and the onset energy of the HOMOs with R^2 values of 0.9228 (Figure 8a) and 0.9258 (Figure 8b), respectively. A comparison between the energy levels of the metal-based frontier orbitals for **III**, **1**, **2**, **3**, and **IV** shows that the relative energy of such orbitals increases from that of the tetraformamidinate paddlewheel compound, **III**, to that of the tetraguanidinate one, **IV**. The large energy range of the HOMO (∼1.5 eV) shows that substitution of $^-$DAniF for $^-$hpp results in a large change in the electronic structure of the paddlewheel compounds. This trend correlates with the ligand donor ability that increases gradually as formamidinates get replaced by the guanidinate hpp. Furthermore, the systematic addition of electron-donating hpp ligands results in a smaller HOMO−LUMO energy gap, thus decreasing the metal character of the δ orbitals (HOMO) due to a greater mixing of metal- and ligand-based orbitals.[55] The magnitude of the half-wave potential for the synthesized compounds follows the order **1** < **2** < **3** based on their HOMO energies as the number of guanidinates are introduced into the system. This observation is in agreement with the obtained electrochemical data, where the destabilization of the Mo_2^{4+} core is reflected in the negative shift of the redox potentials that favors the formation of the M_2^{5+} and M_2^{6+} species.

Density functional theory was used to help assign the ν(Mo−Mo) vibrational modes. Table 4 presents the experimental and calculated Raman shifts of ν(Mo−Mo). We can observe that the frequencies for the dimolybdenum stretch in compounds **1**−**3** are between 487 and 505 cm^{-1}. Compared to the vibration of the tetraacetate moiety, the higher frequency of the vibration for **1**−**3** can be attributed to a smaller Mo−Mo bond and the increase in the metal−metal bond strength.[60] The calculated Raman shifts obtained by DFT show an increase in the frequency for the dimolybdenum stretch as a function of the number of guanidinates being substituted with a correlation coefficient (R^2) of 0.9676 (Figure 8c), consistent with the reduction of the HOMO−LUMO gap. Nonetheless, the difference in the calculated frequencies between compounds **1** and **3** is 21 cm^{-1} (0.06 kcal/mol).

Time-dependent density functional theory calculations were performed on geometry-optimized compounds **1**−**3** to help

https://dx.doi.org/10.1021/acs.inorgchem.9b03394
Inorg. Chem. 2020, 59, 3091−3101

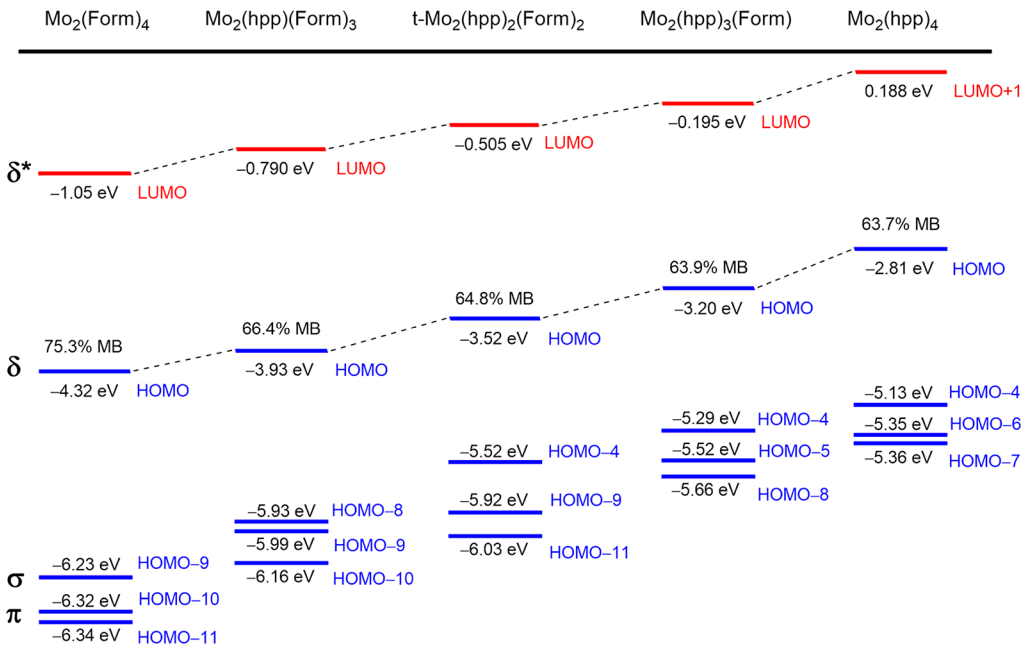

Figure 7. Diagram showing the respective relative energies of the molecular orbitals of **III**, **1**, **2**, **3**, and **IV**. The metal-based character of the δ HOMO orbital is displayed. The blue lines indicate the filled orbitals for all complexes, while the red lines represent their empty orbitals.

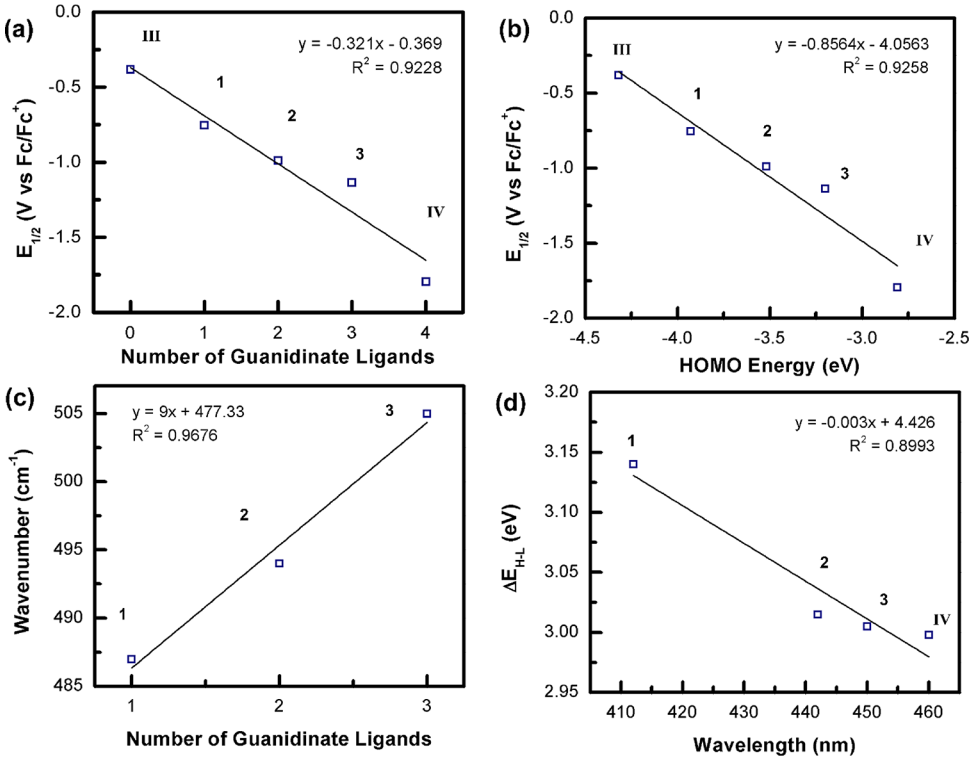

Figure 8. Plot of the dependence of (a) half-wave potentials ($E_{1/2}$) on the number of guanidinates around the Mo_2 core, with zero being the tetraformamidinate (**III**); (b) potential separation ($E_{1/2}$) on the calculated energy of the highest occupied molecular orbitals for **III**, **1**, **2**, **3**, and **IV**; (c) the Raman shifts for the ν(Mo−Mo) stretch on the guanidinate ligands for **1**, **2**, and **3**; and (d) the lowest-energy absorption band associated with the $\delta \rightarrow \delta^*$ electronic transition on the calculated HOMO−LUMO energy gap for **1**, **2**, **3**, and **IV**. The squares are the measured values, and the solid lines are the least-square fits of the data.

assign the lowest-energy transition observed in the UV−vis spectra for each compound. Absorption spectra of **1** shows a band at 412 nm arising from the $\delta \rightarrow \delta^*$ transition. Similarly, **2** presented a band at 442 nm while the same signal appeared at 450 nm for **3**. These bands correspond to the HOMO → LUMO transition calculated to be 520, 542, and 572 nm for **1**, **2**, and **3**, respectively. A bathochromic shift is present in the electronic absorption spectra for these molecules as guanidinates are substituted in the Mo−Mo center, from the tetraformamidinate (**III**) (430 nm) to the tetraguanidinate

https://dx.doi.org/10.1021/acs.inorgchem.9b03394
Inorg. Chem. 2020, 59, 3091−3101

Table 4. Experimental and Calculated Raman Shifts for ν(Mo−Mo)

	experimental (cm^{-1})	calculated (cm^{-1})
I	404	
III	404	407
1	487	489
2	494	492
3	505	510
IV		501

complex (**IV**) (460 nm) as depicted in Figure 8d with a correlation coefficient (R^2) of 0.8993. This feature is attributed to the delocalization of the uncoordinated nitrogen lone pair into the ligand π system, which narrows the HOMO−LUMO energy gap as observed in the calculated relative energies in Figure 7.[61] Meanwhile, the higher-energy transitions observed at 290, 295, and 330 nm for **1**, **2**, and **3**, respectively, were calculated at 375, 362, and 358 nm. These high-energy transitions correspond to the $\delta \rightarrow \pi_M^*$ transition for **1**, $\pi_M \rightarrow \delta^*$ in the case of **2**, and $\delta \rightarrow \pi_L$ for **3**. Experimental and calculated wavelengths for the δ to δ^* transition of **I**, **III**, **1**, **2**, **3**, and **IV** are displayed in Table 5.

Table 5. Experimentally Obtained and Calculated λ_{max} in the Electronic Spectra for I, III, 1, 2, 3, and IV

	experimental (nm)	calculated (nm)
I	303[60]	
III	430[24]	
1	412	520
2	442	542
3	450	572
IV	460[61]	

CONCLUSIONS

A series of quadruply bonded dimolybdenum compounds were successfully synthesized and characterized. Compounds **1** and **2** were structurally characterized by single-crystal X-ray crystallography presenting a Mo−Mo distance of 2.0844(6) and 2.0784(6) Å, respectively. Data obtained from Raman spectroscopy shows an increase in the Raman shift with the addition of guanidinate ligands, 487, 494, and 505 cm^{-1} for **1**, **2**, and **3**, respectively. Electrochemical studies showed that the $Mo_2^{4+/5+}$ redox process can be tuned over a range of nearly 0.4 V due to the increased ligand basicity. In addition, we have shown the ability of hpp to stabilize higher oxidation states for the Mo_2 unit. The addition of two and three guanidinate ligands shows the ability of these complexes to perform multielectron redox chemistry. DFT calculations depict a strong influence on the guanidinate ligand in the difference in energy levels between the compounds. These observations show greater metal−ligand mixing as formamidinates were replaced by guanidinates, thus reducing the metal character of the HOMO. Moreover, the decrease in energy for the $\delta \rightarrow \delta^*$ transition (as guanidinates are introduced into the Mo_2 core) is in agreement with an increase in the d orbital overlap and bond strength, hence shortening the Mo−Mo bond distances.

ASSOCIATED CONTENT

Supporting Information

The Supporting Information is available free of charge at https://pubs.acs.org/doi/10.1021/acs.inorgchem.9b03394.

Selected bond lengths and angles for X-ray-characterized compounds **1** and **2**; ^{1}H NMR for **1**−**3**; calculated and experimentally obtained mass spectra of **1**−**3**; synthesis, X-ray crystallographic data, and *XYZ* coordinates of $[Mo_2(DAniF)_2(hpp)_2](PF_6)$; cyclic voltammograms of **I**, **II**, and **III**; Raman spectra of **I** and **III**; infrared spectra of **2**; and Cartesian coordinates of the DFT-optimized geometries in the gas phase (PDF)

Accession Codes

CCDC 1970116−1970117 and 1979462 contain the supplementary crystallographic data for this paper. These data can be obtained free of charge via www.ccdc.cam.ac.uk/data_request/cif, or by emailing data_request@ccdc.cam.ac.uk, or by contacting The Cambridge Crystallographic Data Centre, 12 Union Road, Cambridge CB2 1EZ, UK; fax: +44 1223 336033.

AUTHOR INFORMATION

Corresponding Author

Dino Villagrán − *Department of Chemistry and Biochemistry, The University of Texas at El Paso, El Paso, Texas 79968, United States*; orcid.org/0000-0002-5798-3584; Email: dino@utep.edu

Authors

Nancy Rodríguez-López − *Department of Chemistry and Biochemistry, The University of Texas at El Paso, El Paso, Texas 79968, United States*

Nathalie Metta − *Department of Chemistry and Biochemistry, The University of Texas at El Paso, El Paso, Texas 79968, United States*

Alejandro J. Metta-Magana − *Department of Chemistry and Biochemistry, The University of Texas at El Paso, El Paso, Texas 79968, United States*

Complete contact information is available at: https://pubs.acs.org/10.1021/acs.inorgchem.9b03394

Notes

The authors declare no competing financial interest.

ACKNOWLEDGMENTS

We thank Prof. Luis Echegoyen for access to the Raman spectrometer. N.R.-L. acknowledges financial support from CONACYT (Consejo Nacional de Ciencia y Tecnología) México. We acknowledge the NSF-MRI program (CHE-1827875) for the funding to purchase an X-ray diffractometer.

REFERENCES

(1) Cotton, F. A.; Gruhn, N. E.; Gu, J.; Huang, P.; Lichtenberger, D. L.; Murillo, C. A.; Dorn, L. O. V.; Wilkinson, C. C. Closed-Shell Molecules That Ionize More Readily Than Cesium. *Science* **2002**, *298* (5600), 1971−1974.

(2) Lin, C.; Protasiewicz, J. D.; Smith, E. T.; Ren, T. Redox Tuning of the Dimolybdenum Compounds at the Ligand Periphery: A Direct Correlation with the Hammett Constant of the Substituents. *J. Chem. Soc., Chem. Commun.* **1995**, No. 22, 2257−2258.

(3) Ventura, K.; Prat, J. R.; Quintana, L. M. A.; Goos, A.; Villagran, D. Unprecedented $W_2(0)$ Quadruply Bonded Complex Supported by π-Donor Ligands. *Chem. Commun.* **2016**, *52* (20), 3974−3976.
(4) Cotton, F. A.; Gu, J.; Murillo, C. A.; Timmons, D. J. The First Dinuclear Complex of Palladium(III). *J. Am. Chem. Soc.* **1998**, *120* (50), 13280−13281.
(5) Cotton, F. A.; Murillo, C. A.; Timmons, D. J.; Murillo, C. A. First Paddlewheel Complex with a Doubly-Bonded Ir_2^{6+} Core. *Chem. Commun.* **1999**, No. 15, 1427−1428.
(6) Chiarella, G. M.; Cotton, F. A.; Murillo, C. A. An Uncommon Highly Oxidized Multiple Bonded Re_2^{8+} Species. *Chem. Commun.* **2011**, *47* (31), 8940−8942.
(7) Cotton, F. A.; Matonic, J. H.; Murillo, C. A. A New Type of Divalent Niobium Compound: The First Nb−Nb Triple Bond in a Tetragonal Lantern Environment. *J. Am. Chem. Soc.* **1997**, *119* (33), 7889−7890.
(8) Cotton, F. A.; Daniels, L. M.; Murillo, C. A.; Timmons, D. J.; Wilkinson, C. C. The Extraordinary Ability of Guanidinate Derivatives to Stabilize Higher Oxidation Numbers in Dimetal Units by Modification of Redox Potentials: Structures of Mo_2^{5+} and Mo_2^{6+} Compounds. *J. Am. Chem. Soc.* **2002**, *124* (31), 9249−9256.
(9) Cotton, F. A.; Donahue, J. P.; Gruhn, N. E.; Lichtenberger, D. L.; Murillo, C. A.; Timmons, D. J.; Van Dorn, L. O.; Villagrán, D.; Wang, X. Facilitating Access to the Most Easily Ionized Molecule: An Improved Synthesis of the Key Intermediate, $W_2(hpp)_4Cl_2$, and Related Compounds. *Inorg. Chem.* **2006**, *45* (1), 201−213.
(10) Chiarella, G. M.; Cotton, F. A.; Dalal, N. S.; Murillo, C. A.; Wang, Z.; Young, M. D. Direct Evidence from Electron Paramagnetic Resonance for Additional Configurations in Uncommon Paddlewheel Re_2^{7+} Units Surrounded by an Unsymmetrical Bicyclic Guanidinate. *Inorg. Chem.* **2012**, *51* (9), 5257−5263.
(11) Cotton, F. A.; Dalal, N. S.; Huang, P.; Murillo, C. A.; Stowe, A. C.; Wang, X. The First Structurally Confirmed Paddlewheel Compound with an M_2^{7+} Core: $[Os_2(hpp)_4Cl_2](PF_6)$. *Inorg. Chem.* **2003**, *42* (3), 670−672.
(12) Bear, J. L.; Li, Y.; Han, B.; Kadish, K. M. Synthesis, Molecular Structure, and Electrochemistry of a Paramagnetic Diruthenium(III) Complex. Characterization of $Ru_2(hpp)_4Cl_2$, Where Hpp Is the 1,3,4,6,7,8- Hexahydro-2H-Pyrimido[1,2-a]Pyrimidinate Ion. *Inorg. Chem.* **1996**, *35* (5), 1395−1398.
(13) Novak, I.; Wei, X.; Chin, W. S. Electronic Structures of Very Strong, Neutral Bases. *J. Phys. Chem. A* **2001**, *105* (10), 1783−1788.
(14) Bailey, P. J.; Pace, S. The Coordination Chemistry of Guanidines and Guanidinates. *Coord. Chem. Rev.* **2001**, *214* (1), 91−141.
(15) Cotton, F. A.; Donahue, J. P.; Lichtenberger, D. L.; Murillo, C. A.; Villagrán, D. Expeditious Access to the Most Easily Ionized Closed-Shell Molecule, $W_2(hpp)_4$. *J. Am. Chem. Soc.* **2005**, *127* (31), 10808−10809.
(16) Chiarella, G. M.; Cotton, F. A.; Durivage, J. C.; Lichtenberger, D. L.; Murillo, C. A. Solubilizing the Most Easily Ionized Molecules and Generating Powerful Reducing Agents. *J. Am. Chem. Soc.* **2013**, *135* (47), 17889−17896.
(17) Berry, J. F.; Bothe, E.; Cotton, F. A.; Ibragimov, S. A.; Murillo, C. A.; Villagrán, D.; Wang, X. Metal−Metal Bonding in Mixed Valence Ni_2^{5+} Complexes and Spectroscopic Evidence for a Ni_2^{6+} Species. *Inorg. Chem.* **2006**, *45* (11), 4396−4406.
(18) Cotton, F. A.; Murillo, C. A.; Wang, X.; Wilkinson, C. C. Increasing the Solubility of Strong Reducing Agents Containing Mo_2^{4+} Units and Alkyl-Substituted Guanidinate Ligands. *Dalton Trans.* **2007**, *0* (35), 3943−3951.
(19) Cotton, F. A.; Murillo, C. A.; Wang, X.; Wilkinson, C. C. Homologues of the Easily Ionized Compound $Mo_2(hpp)_4$ Containing Smaller Bicyclic Guanidinates. *Inorg. Chem.* **2006**, *45* (14), 5493−5500.
(20) Chiarella, G. M.; Cotton, F. A.; Murillo, C. A.; Young, M. D. Tuning the Electrochemistry of Re_2^{6+} Species with Divergent Bicyclic Guanidinate Ligands and by Modification of Axial π Interactions. *Inorg. Chem.* **2011**, *50* (4), 1258−1264.
(21) Cotton, F. A.; Liu, C. Y.; Murillo, C. A. Systematic Preparation of Mo_2^{4+} Building Blocks for Supramolecular Assemblies. *Inorg. Chem.* **2004**, *43* (7), 2267−2276.
(22) Chisholm, M. H.; Cotton, F. A.; Daniels, L. M.; Folting, K.; Huffman, J. C.; Iyer, S. S.; Lin, C.; Macintosh, A. M.; Murillo, C. A. Compounds in Which the Mo_2^{4+} Unit Is Embraced by One, Two or Three Formamidinate Ligands Together with Acetonitrile Ligands. *J. Chem. Soc., Dalton Trans.* **1999**, *0* (9), 1387−1392.
(23) *Multiple Bonds between Metal Atoms*, 3rd ed.; Cotton, F. A., Murillo, C. A., Walton, R. A., Eds.; Springer-Verlag: New York, 2005.
(24) Bradley, W.; Wright, I. 129. Metal Derivatives of NN′-Diarylamidines. *J. Chem. Soc.* **1956**, *0* (0), 640−648.
(25) Cotton, F. A.; Daniels, L. M.; Murillo, C. A.; Slaton, J. G. A Pseudo-Jahn−Teller Distortion in an $Mo_2(M_2\text{-}O)_2$ Ring Having the Shortest MoIV−MoIV Double Bond. *J. Am. Chem. Soc.* **2002**, *124* (12), 2878−2879.
(26) Cotton, F. A.; Liu, C. Y.; Murillo, C. A.; Villagrán, D.; Wang, X. Modifying Electronic Communication in Dimolybdenum Units by Linkage Isomers of Bridged Oxamidate Dianions. *J. Am. Chem. Soc.* **2003**, *125* (44), 13564−13575.
(27) Lin, C.; Protasiewicz, J. D.; Smith, E. T.; Ren, T. Linear Free Energy Relationships in Dinuclear Compounds. 2. Inductive Redox Tuning via Remote Substituents in Quadruply Bonded Dimolybdenum Compounds. *Inorg. Chem.* **1996**, *35* (22), 6422−6428.
(28) Becke, A. D. Density-functional Thermochemistry. III. The Role of Exact Exchange. *J. Chem. Phys.* **1993**, *98* (7), 5648−5652.
(29) Lee, C.; Yang, W.; Parr, R. G. Development of the Colle-Salvetti Correlation-Energy Formula into a Functional of the Electron Density. *Phys. Rev. B: Condens. Matter Mater. Phys.* **1988**, *37* (2), 785−789.
(30) Frisch, M. J.; Trucks, G. W.; Schlegel, H. B.; Scuseria, G. E.; Robb, M. A.; Cheeseman, J. R.; Scalmani, G.; Barone, V.; Mennucci, B.; Petersson, G. A.; Nakatsuji, H.; Caricato, M.; Li, X.; Hratchian, H. P.; Izmaylov, A. F.; Bloino, J.; Zheng, G.; Sonnenberg, J. L.; Hada, M.; Ehara, M.; Toyota, K.; Fukuda, R.; Hasegawa, J.; Ishida, M.; Nakajima, T.; Honda, Y.; Kitao, O.; Nakai, H.; Vreven, T.; Montgomery, J. A.; Peralta, J. E.; Ogliaro, F.; Bearpark, M.; Heyd, J. J.; Brothers, E.; Kudin, K. N.; Staroverov, V. N.; Kobayashi, R.; Normand, J.; Raghavachari, K.; Rendell, A.; Burant, J. C.; Iyengar, S. S.; Tomasi, J.; Cossi, M.; Rega, N.; Millam, J. M.; Klene, M.; Knox, J. E.; Cross, J. B.; Bakken, V.; Adamo, C.; Jaramillo, J.; Gomperts, R.; Stratmann, R. E.; Yazyev, O.; Austin, A. J.; Cammi, R.; Pomelli, C.; Ochterski, J. W.; Martin, R. L.; Morokuma, K.; Zakrzewski, V. G.; Voth, G. A.; Salvador, P.; Dannenberg, J. J.; Dapprich, S.; Daniels, A. D.; Farkas, Ö.; Foresman, J. B.; Ortiz, J. V.; Cioslowski, J.; Fox, D. J.; *Gaussian 09*, Revision C.01; Gaussian Inc.: Wallingford CT, 2010.
(31) Dunning, T. H. Gaussian Basis Sets for Use in Correlated Molecular Calculations. I. The Atoms Boron through Neon and Hydrogen. *J. Chem. Phys.* **1989**, *90* (2), 1007−1023.
(32) Kendall, R. A.; Dunning, T. H.; Harrison, R. J. Electron Affinities of the First-row Atoms Revisited. Systematic Basis Sets and Wave Functions. *J. Chem. Phys.* **1992**, *96* (9), 6796−6806.
(33) Woon, D. E.; Dunning, T. H. Gaussian Basis Sets for Use in Correlated Molecular Calculations. III. The Atoms Aluminum through Argon. *J. Chem. Phys.* **1993**, *98* (2), 1358−1371.
(34) Peterson, K. A.; Woon, D. E.; Dunning, T. H. Benchmark Calculations with Correlated Molecular Wave Functions. IV. The Classical Barrier Height of the $H+H_2 \rightarrow H_2+H$ Reaction. *J. Chem. Phys.* **1994**, *100* (10), 7410−7415.
(35) Wilson, A. K.; van Mourik, T.; Dunning, T. H. Gaussian Basis Sets for Use in Correlated Molecular Calculations. VI. Sextuple Zeta Correlation Consistent Basis Sets for Boron through Neon. *J. Mol. Struct.: THEOCHEM* **1996**, *388*, 339−349.
(36) Dunning, T. H.; Hay, P. J. Gaussian Basis Sets for Molecular Calculations. In *Methods of Electronic Structure Theory*; Schaefer, H. F., Ed.; Modern Theoretical Chemistry; Springer US: Boston, 1977; pp 1−27.

https://dx.doi.org/10.1021/acs.inorgchem.9b03394
Inorg. Chem. 2020, 59, 3091−3101

(37) Hay, P. J.; Wadt, W. R. Ab Initio Effective Core Potentials for Molecular Calculations. Potentials for the Transition Metal Atoms Sc to Hg. *J. Chem. Phys.* **1985**, *82* (1), 270−283.
(38) Wadt, W. R.; Hay, P. J. Ab Initio Effective Core Potentials for Molecular Calculations. Potentials for Main Group Elements Na to Bi. *J. Chem. Phys.* **1985**, *82* (1), 284−298.
(39) Hay, P. J.; Wadt, W. R. Ab Initio Effective Core Potentials for Molecular Calculations. Potentials for K to Au Including the Outermost Core Orbitals. *J. Chem. Phys.* **1985**, *82* (1), 299−310.
(40) Bauernschmitt, R.; Ahlrichs, R. Treatment of Electronic Excitations within the Adiabatic Approximation of Time Dependent Density Functional Theory. *Chem. Phys. Lett.* **1996**, *256* (4), 454−464.
(41) Casida, M. E.; Jamorski, C.; Casida, K. C.; Salahub, D. R. Molecular Excitation Energies to High-Lying Bound States from Time-Dependent Density-Functional Response Theory: Characterization and Correction of the Time-Dependent Local Density Approximation Ionization Threshold. *J. Chem. Phys.* **1998**, *108* (11), 4439−4449.
(42) Stratmann, R. E.; Scuseria, G. E.; Frisch, M. J. An Efficient Implementation of Time-Dependent Density-Functional Theory for the Calculation of Excitation Energies of Large Molecules. *J. Chem. Phys.* **1998**, *109* (19), 8218−8224.
(43) Van Caillie, C.; Amos, R. D. Geometric Derivatives of Excitation Energies Using SCF and DFT. *Chem. Phys. Lett.* **1999**, *308* (3), 249−255.
(44) Van Caillie, C.; Amos, R. D. Geometric Derivatives of Density Functional Theory Excitation Energies Using Gradient-Corrected Functionals. *Chem. Phys. Lett.* **2000**, *317* (1), 159−164.
(45) Scalmani, G.; Frisch, M. J.; Mennucci, B.; Tomasi, J.; Cammi, R.; Barone, V. Geometries and Properties of Excited States in the Gas Phase and in Solution: Theory and Application of a Time-Dependent Density Functional Theory Polarizable Continuum Model. *J. Chem. Phys.* **2006**, *124* (9), 094107.
(46) Furche, F.; Ahlrichs, R. Adiabatic Time-Dependent Density Functional Methods for Excited State Properties. *J. Chem. Phys.* **2002**, *117* (16), 7433−7447.
(47) Cotton, F. A.; Daniels, L. M.; Hillard, E. A.; Murillo, C. A. The Lengths of Molybdenum to Molybdenum Quadruple Bonds: Correlations, Explanations, and Corrections. *Inorg. Chem.* **2002**, *41* (9), 2466−2470.
(48) Lawton, D.; Mason, R. The Molecular Structure of Molybdenum(II) Acetate. *J. Am. Chem. Soc.* **1965**, *87* (4), 921−922.
(49) Tanaka, S.; Mashima, K. Unique Stepwise Substitution Reaction of a Mono(Guanidinate)Tetraplatinum Complex with Amidines, Giving Mono(Amidinate)Tetraplatinum Complexes through Mixed- Ligand Intermediate Complexes. *Dalton Trans.* **2013**, *42* (8), 2831−2840.
(50) Chifotides, H. T.; Catalan, K. V.; Dunbar, K. R. Dirhodium Formamidinate Compounds with Bidentate Nitrogen Chelating Ligands. *Inorg. Chem.* **2003**, *42* (26), 8739−8747.
(51) Cotton, F. A.; Lin, C.; Murillo, C. A. Maximum Communication between Coupled Oxidations of Dimetal Units. *J. Am. Chem. Soc.* **2001**, *123* (11), 2670−2671.
(52) Bailey, P. J.; Bone, S. F.; Mitchell, L. A.; Parsons, S.; Taylor, K. J.; Yellowlees, L. J. A New Bridging Ligand for the $[Mo_2]^{4+}$ Dimer: Syntheses and X-Ray Crystal Structures of the Redox Pair $[Mo_2\{\mu\text{-}H_2\text{-}(NPh)_2CNHPh\}_4]^{0/+}$. *Inorg. Chem.* **1997**, *36* (5), 867−871.
(53) Cai, X.-M.; Zimmermann, T. K.; Pöthig, A.; Kühn, F. E. Synthesis and Electrochemical Properties of Cis- and Trans-$[Mo_2(O_2C\text{-}Fc)_2(DArF)_2]$ (O_2C-Fc = Ferrocenecarboxylate; DArF = N,N′-Diarylformamidinate). *Inorg. Chem.* **2015**, *54* (13), 6631−6640.
(54) Cotton, F. A.; Kühn, F. E. Syntheses and Structures of Di(Carboxylato)Hexakis(Acetonitrile)-Dimolybdenum(II) Bis-(Tetrafluoroborate) and Trans-[Di(μ-Acetato)-Di(Acetonitrile)Di-(μ-Bis(Diphenylphosphino)Amine)Dimolybdenum(II)] Bis-(Tetrafluoroborate). *Inorg. Chim. Acta* **1996**, *252* (1), 257−264.
(55) Hicks, J.; Ring, S. P.; Patmore, N. J. Tuning the Electronic Structure of Mo−Mo Quadruple Bonds by N for O for S Substitution. *Dalton Trans.* **2012**, *41* (22), 6641−6650.
(56) Ketteringham, A. P.; Oldham, C. Raman Spectra of Multiply Bonded Metal Species. *J. Chem. Soc., Dalton Trans.* **1973**, *0* (10), 1067−1070.
(57) Ventura, K.; Veleta, J. M.; Metta-Magaña, A.; Villagrán, D. Stabilization of a W_2^{6+} Bimetallic Complex Supported by Two N,N′,N″-Triphenylguanidinate Ligands. *Inorg. Chim. Acta* **2015**, *424*, 286−292.
(58) Minenkov, Y.; Singstad, Å.; Occhipinti, G.; Jensen, V. R. The Accuracy of DFT-Optimized Geometries of Functional Transition Metal Compounds: A Validation Study of Catalysts for Olefin Metathesis and Other Reactions in the Homogeneous Phase. *Dalton Trans.* **2012**, *41* (18), 5526−5541.
(59) Chisholm, M. H.; Gallucci, J.; Hadad, C. M.; Huffman, J. C.; Wilson, P. J. $M_2(hpp)_4Cl_2$ and $M_2(hpp)_4$, Where M = Mo and W: Preparations, Structure and Bonding, and Comparisons with C_2, C_2H_2, and C_2Cl_2 and the Hypothetical Molecules $M_2(hpp)_4(H)_2$. *J. Am. Chem. Soc.* **2003**, *125* (51), 16040−16049.
(60) Acho, J. A.; Ren, T.; Yun, J. W.; Lippard, S. J. Dimolybdenum-(II) Calixarene Complexes: Synthesis, Structure, Raman Spectroscopy, and Bonding. *Inorg. Chem.* **1995**, *34* (21), 5226−5233.
(61) Thomas, M. B.; Jindasa, R. G. W.; Hu, Y.; Schmitz, B.; Wang, H.; D'Souza, F. Investigation of the Push−Pull Effects on β-Functionalized Zinc Porphyrin Coordinated to C_{60} Donor−Acceptor Conjugates. *Can. J. Chem.* **2018**, *96* (9), 881−889.

https://dx.doi.org/10.1021/acs.inorgchem.9b03394
Inorg. Chem. 2020, 59, 3091−3101